CrossMark

Plastic collapse of lattice structures under a general stress state

Babak Haghpanah, Jim Papadopoulos, Ashkan Vaziri *

Department of Mechanical and Industrial Engineering, Northeastern University, Boston, MA, USA

A B S T R A C T

We present a numerical minimization procedure to determine the macroscopic 'plastic collapse strength' of a tessellated cellular structure under a general stress state. The method is illustrated with sample cellular structures of regular and hierarchical honeycombs. Based on the deformation modes found by minimization of plastic dissipation, closed-form expressions for strength are derived. The current work generalizes previous studies on plastic collapse analysis of lattice structures, which are limited to very simple loading conditions.

1. Introduction

Strength and energy absorption capacity of lattice structures are governed by buckling of the cell walls or plastic yielding of cell wall material (Evans et al., 2001; Evans et al., 1998; Ashby, 2006; Papka and Kyriakides, 1994; Jang and Kyriakides, 2009; Babaee et al., 2012). However, the current state of the literature on collapse of cellular lattice structures is limited to structures subjected to simple loading conditions such as uniaxial, biaxial or shear loading applied at special orientations (Gibson et al., 1989; Gibson et al., 1982; Haghpanah et al., 2013; Onck et al., 2001; Karagiozova and Yu, 2004; Zhu and Mills, 2000). In this article, we focus on plastic deformation, and present a method that allows numerical and algebraic calculation of plastic collapse strength under arbitrary states of stress or strain. The presented method is based on minimizing the internal plastic dissipation inside a unit cell of the tessellated structure (Chen et al., 2007). To illustrate the method, two two-dimensional networks of rigid-plastic beams are considered. First, a hexagonal network (*honeycomb*) with sixfold rotational symmetry, and second, the first iteration of the honeycomb structure in a hierarchical refinement scheme in which all three–edge nodes are replaced with smaller, parallel hexagons defined by size ratio γ, with $\gamma = 0$ denoting a regular honeycomb. The latter structure, also maintaining a microscopic sixfold symmetry, is called *first order hierarchical honeycomb* (Ajdari et al., 2012), see Fig. 1. The relations between macroscopic stress and strain states and unit cell reaction forces and displacements, respectively, are derived in Section 2 in a convenient canonical position which is suitable for threefold symmetrical structures. The minimization of plastic dissipation inside the unit cell subjected to external forces or displacements is detailed in Section 3. We then exploit the observed unit-cell deformation patterns to derive analytical expressions for strength, to permit efficient computation and plotting. The results from the minimization scheme and also the derived upper bounds of plastic collapse are presented in Section 4. Lastly in Section 5, a summary of the current work and conclusions are given.

2. Threefold definitions of stress and strain

We begin our analysis with threefold symmetric definitions of both microscopic and macroscopic stress and strain (note that for structures without a threefold symmetry (e.g. square honeycomb) the conventional Cartesian coordinate system can be used readily). To carry out the

---

* Corresponding author. Tel.: +1 6172706813.
E-mail address: vaziri@coe.neu.edu (A. Vaziri).
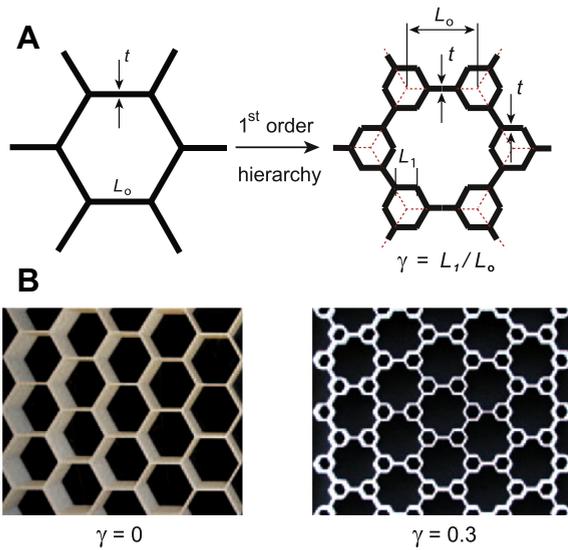
Fig. 1. (A) Schematics of regular and hierarchical honeycombs with one level of hierarchy. (B) Images of *regular* and *hierarchical* ($\gamma = 0.3$) honeycombs with $L_0 = 2$ cm fabricated using three-dimensional printing.

analyses we select a *unit cell*, with associated tractions and displacements, which tiles the plane to represent the loaded lattice structure. The structural unit cell for our hexagonal-based patterns encompasses one vertex of the original hexagonal network, out to the midpoints of the original hexagon sides (a distance $L_0/2$), see Fig. 2(A). The area associated with the unit cell is a triangle joining the three hexagon center-points that surround this vertex, with area $3\sqrt{3}L_0^2/4$. The general state of stress is expressed in terms of its normal components in the three in-plane material directions $a = 0°$, $b = 120°$ and $c = 240°$: σ_{aa}, σ_{bb}, σ_{cc}. Given those three normal components, the xy stress tensor can be written:

$$\begin{bmatrix} \sigma_{xx} & \tau_{xy} \\ \tau_{xy} & \sigma_{yy} \end{bmatrix} = \begin{bmatrix} \sigma_{aa} & \frac{\sigma_{cc}-\sigma_{bb}}{\sqrt{3}} \\ \frac{\sigma_{cc}-\sigma_{bb}}{\sqrt{3}} & \frac{2\sigma_{cc}+2\sigma_{bb}-\sigma_{aa}}{3} \end{bmatrix} \tag{1}$$

where x and y axes are taken along the so-called armchair (or ribbon) and zigzag (or transverse) directions.

We then examine the allowable external loads at numbered points 1, 4, 7 of the unit cell shown in Fig. 2(B). First we argue that there are no moments applied at these points: the 180° rotational symmetry of the tessellated structure (and trivially the components of microscopic stress) means that any upwards curvature at such a point must become downwards curvature after the rotation, and the only way these can be equal is to have the value zero. Then, using the vertical cut line Δ_a which intersects horizontal sides with a spacing $L_0\sqrt{3}$, we deduce the value of radial force F_a to be $\sigma_{aa}L_0\sqrt{3}$, and similarly for radial directions b, c. Note also that the arbitrary radial forces F_a, F_b, F_c will not be in equilibrium so there must be transverse forces G_a, G_b, G_c, defined as positive counter-clockwise about the origin. Successively taking moments of forces about pairwise intersections of G_a, G_b, G_c, we find $G_a = (F_c - F_b)/\sqrt{3}$, and cyclically.

Next, we consider relations between macroscopic strain and relative displacements of the unit cell boundary points. Given arbitrary radial and tangential displacements of points 1, 4, 7, we can use rigid body displacements and rotation to place the deformed unit cell uniquely in a *canonical position* with the boundary points 1, 4, 7 still on the a, b, c lines. In that unique placement, the boundary point *canonical radial displacements* along the a, b, c lines are named δ_a, δ_b, δ_c, where the segments 1–2, 4–5, 8–7 are generally no longer parallel to those lines. Since the boundary loads are in equilibrium, the introduced rigid body displacements and rotations do not affect the net work.

Given δ_a, the strain is uniaxial along a. Its magnitude is the change in the unit cell x dimension divided by the original unit cell x dimension $3L_0/4$, in other words $\epsilon_a = 4\delta_a/3L_0$. Purely uniaxial strains in all three directions can be superposed to define a general xy strain tensor:

$$\begin{bmatrix} \epsilon_{xx} & \epsilon_{xy} \\ \epsilon_{xy} & \epsilon_{yy} \end{bmatrix} = \begin{bmatrix} \frac{4\delta_a+\delta_b+\delta_c}{3L_0} & \frac{\sqrt{3}(\delta_c-\delta_b)}{3L_0} \\ \frac{\sqrt{3}(\delta_c-\delta_b)}{3L_0} & \frac{\delta_b+\delta_c}{L_0} \end{bmatrix} \tag{2}$$
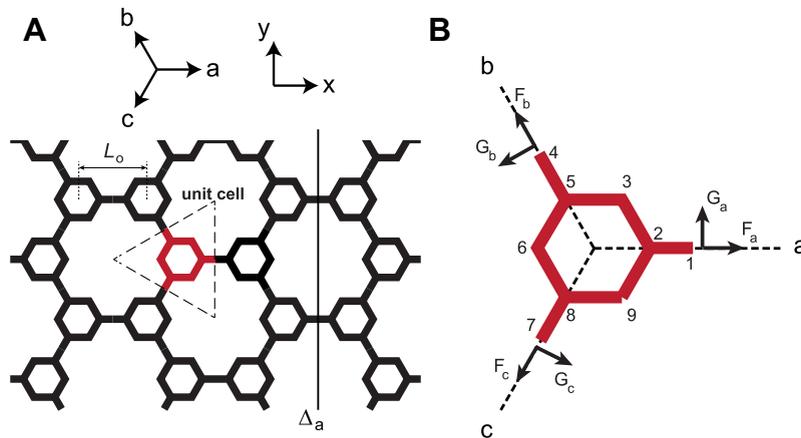
Fig. 2. (A) Schematic of a hierarchical honeycomb where a unit cell of the structure is marked by red lines, (B) free body diagram of the unit cell of hierarchical honeycomb.

It can be shown that the contraction of stress with strain, times unit cell area, times cell wall depth, equals $F_a\delta_a + F_b\delta_b + F_c\delta_c$, namely the work done on the unit cell as it deforms. Transverse boundary forces do no net work since transverse boundary displacements are zero.

3. Plastic collapse strength estimation

3.1. Numerical minimization of plastic work

According to the upper bound theory of plasticity, the actual internal deformations of a rigid-plastic structure subjected to given external displacements must minimize the internal plastic work (Chen et al., 2007). In a network of beams under macroscopic stress, all beams have the maximum bending moment, and therefore the possibility of a plastic hinge, only at their ends. Thus, for a 2D structure the degrees of freedom may be taken as the displacements x_i, y_i and rotations N_i of each node i. The rotation of each rigid-plastic beam connecting nodes i and j can be defined uniquely from its end displacements as $\vec{R}_{ij} = \hat{u}_{ij} \times \vec{D}_{ij}/L_{ij}$, where $\hat{u}_{ij}$ is the beam unit vector pointing from node i to node j, $\vec{D}_{ij}$ is the vector displacement of node j relative to node i, and L_{ij} is beam length. Stretching is determined as $\hat{u}_{ij} \cdot \vec{D}_{ij}$.

The stretching work per unit depth for a beam of thickness t and length L_{ij} connecting nodes i and j with material yield strength σ_Y is calculated as $\sigma_Y t |\hat{u}_{ij} \cdot \vec{D}_{ij}|$. We suppress axial strain in our structure by elevating the axial collapse strength, $\sigma_Y t$, to about $1E6$ times the plastic limit moment divided by beam length, $\sigma_Y t^2/4L_{ij}$. Therefore, the dissipation of interest is that at plastic hinges, which exist wherever a beam rotates differently from an adjoining node. If node i is the junction of three beams with rotations R_{ij}, R_{ik} and R_{il} (as at nodes 2, 5 and 8), the plastic dissipation at node i can be calculated as $W_i = M_o * (|N_i - R_{ij}| + |N_i - R_{ik}| + |N_i - R_{il}|)$ where M_o is the plastic limit moment of the beam cross section. The nodal rotations minimizing dissipation at a three-beam joint of equal plastic hinge moment can be determined locally as $N_i = median(R_{ij}, R_{ik}, R_{il})$. For nodes that are junctions of just two beams of equal plastic hinge moment with rotations R_{ij}, R_{ik} (i.e. nodes 3, 6 and 9), the rotation of the node that minimizes the plastic dissipation is equal to the rotation of either beam (or to any rotation between those values), and $W_i = M_o|R_{ij} - R_{ik}|$. Rotations of nodes 1, 4 and 7 are equal to rotations of beam 1–2, 4–5 and 7–8, respectively since there is no bending moment.

After eliminating nodal rotations as variables, the unit cell of a regular honeycomb with fixed radial displacements, δ_a, δ_b, δ_c, has only two degrees of freedom: the x and y displacements of the center node. When a first order of hierarchy is added, the twelve x_i, y_i displacements of six internal nodes (i.e. nodes 2, 3, 5, 6, 8 and 9 in Fig. 2(A)) suffice to compute the plastic work. Collapse strength analysis proceeds as follows: define three radial boundary displacements δ_a, δ_b, δ_c. Minimize the total dissipation over the internal degrees of freedom to find W^P_{min}. Since $W^P_{min} = F_a\delta_a + F_b\delta_b + F_c\delta_c$, (where the displacements are known), possible failure loadings (F_a, F_b, F_c) are points on

a plane in (F_a, F_b, F_c) space, with intercepts $F_a = W^P_{min}/\delta_a$, etc. The envelope of sufficiently many of these planes constitutes the convex failure surface. The above statements apply equally to the stress and strain components σ_{aa} and ϵ_{aa}, etc., since these are proportional to F_a and δ_a, etc.

Unfortunately this displacement-based approach is not well adapted to the somewhat different problem of defining a ratio between load components – a desired direction in radial force or normal stress space – and finding the loading magnitude along that direction that causes collapse. For determining the strength where normal stresses (or equivalently, F_a, F_b, F_c) are applied to the structural unit cell, a different approach may be employed. Now consider that forces F_a, F_b, F_c, or more accurately forces exactly proportional to these (i.e., $\lambda F_a, \lambda F_b, \lambda F_c$, where λ is a dimensionless multiplier) are applied, and the value of λ is sought at which failure occurs. This represents a force vector of known direction but indeterminate magnitude in *abc* space, and the task is to determine the value of the multiplier that will put the vector tip on the failure surface. If we explored all choices for δ_a, δ_b, δ_c, and used the linear relations of the previous paragraph to solve for λ from each W^P_{min} (i.e. finding the λ value putting the force vector on various failure-surface tangent planes) it is clear that the correct value of λ must be the least to be found by this approach. That is because the minimum length of the vector along $\boldsymbol{F} = (F_a, F_b, F_c)$, ending on a tangent plane, occurs when that plane is tangent at the intersection of $\lambda\boldsymbol{F}$ with the failure surface. We therefore seek $\lambda_{min} = \min(W/(F_a\delta_a + F_b\delta_b + F_c\delta_c))$, where the minimization is not only over the twelve internal variables x_i, y_i as previously, but also over the additional variables δ_a, δ_b, δ_c. Note, however, that the minimized quotient is homogeneous of zero order in the δ vector, so a unique answer requires some kind of normalization (for simplicity, we take $\delta_a = 1$). Once λ_{min} is found, $\lambda_{min}\boldsymbol{F}$ may be taken as a point on the failure surface. To perform this minimization in MATLAB, where both the twelve interior displacements and the three external radial displacements are variables, the *fminsearch* subroutine was used. Since the absolute value function $|f|$ essential to the evaluation of plastic work has slope discontinuities making convergence difficult, we adopted the expedient of approximating it by a sequence of smooth functions $|f|^\alpha$, where α is reduced incrementally from 2 to 1 in a hundred steps, and the result of each step becomes starting point for the next.

In Fig. 3 isometric views of plastic collapse surface in the $\bar{\sigma}_{aa}$ $\bar{\sigma}_{bb}$, $\bar{\sigma}_{cc}$ space for regular and hierarchical ($\gamma = 0.5$) honeycombs obtained from the numerical analysis are shown. The plots provide enough data for prediction of plastic collapse strength of the structures under arbitrary 2D loading conditions. Towards this goal, the geometry of 2D stress states in the *abc* space deserves mention. It is well known that the principal stresses $S_1 > S_2$ of arbitrary orientation, θ, map onto Mohr's circle in the σ_{xx}, σ_{yy}; τ_{xy} space. Similarly, they map onto a circle parameterized by θ in the σ_{aa}, σ_{bb}, σ_{cc} space. The origin of this circle is a distance $\sqrt{3}(S_1 + S_2)/2$ along the $(1, 1, 1)$ *hydrostatic* axis. The circle lies in a *deviatoric* plane perpendicular to $(1, 1, 1)$ direction and has a radius of $\sqrt{3}(S_1 - S_2)/\sqrt{8}$. When hydrostatic loading is tensile, the angle defined by three points: (1) the
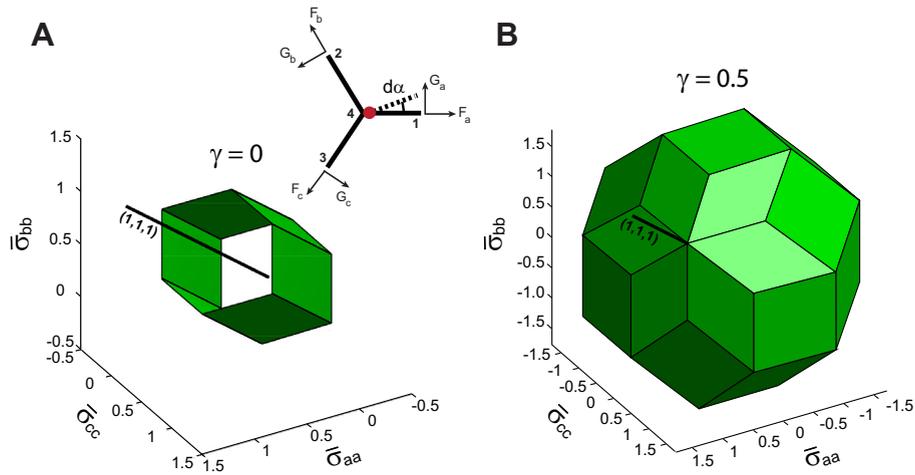
Fig. 3. Plastic collapse surface in the *abc* stress space for (A) regular ($\gamma = 0$) and (B) hierarchical honeycomb ($\gamma = 0.5$). Stresses are normalized according to $\bar{\sigma} = (\sigma/\sigma_Y)/(t/L_0)^2$. The solid lines ($\bar{\sigma}_a = \bar{\sigma}_b = \bar{\sigma}_c$) represent the equi–biaxial state of stress in the *abc* space. The inset shows the plastic deformation mechanism for the unit cell of a regular honeycomb.

mapped point on the circle corresponding to state of stress; (2) the origin of the circle; and (3) the closest point on the circle to the positive σ_{aa} axis, is equal to -2θ, where θ is the angle in *xy* space between the greatest principal stress (S_1) and *x* (or *a*) axis. In general any fixed proportion between principal stresses S_1, S_2 (e.g., $S_2/S_1 = 0$ implies uniaxial stress) represents a cone from the origin, centered along the $(1, 1, 1)$ axis with a vertex half angle of $\arctan\left(3/(2\sqrt{2}) \times |(S_2 - S_1)/(S_2 + S_1)|\right)$.

3.2. Upper bound estimation of plastic collapse

While the numerical results can be used for direct construction of the failure surface, the observed deformation modes can be also used to derive analytical formulae of collapse strength. For regular and hierarchical honeycombs, the modes of deformation found numerically for different geometries and many loadings were examined. Each collapse mechanism turned out to be a single degree of freedom bar-hinge mechanism, with only enough hinges to permit deformation. With an expectation that these modes are the only ones to be activated by any loading, we algebraically calculated the external work for each deformation mode under arbitrary loading, and used the equality of external and internal work to give a relation between load components at failure. The inner envelope of these algebraic relations provides the failure surface.

For a regular honeycomb structure the plastic deformation mechanisms involve one plastic hinge at the inner end of any of the three beams constituting the unit cell. Inset of Fig. 3(A) shows the deformed shape of a unit cell with one plastic hinge at the inner end of the beam along $0°$. By equating the expression of plastic dissipation at a hinge, $\sigma_Y t^2/4 \times d\alpha$, to external work, $|F_c - F_b|/\sqrt{3} \times L_0/2 \times d\alpha$, the external forces causing collapse must satisfy $|F_c - F_b| = \sqrt{3}/2 \times \sigma_Y \times bt^2/L_0$. Repeating this procedure for the two other beams, the set of equations for plastic collapse of the regular honeycomb structure is that any

one of $|F_a - F_b|$, $|F_a - F_c|$, $|F_b - F_c|$ equals $\sqrt{3}/2 \times \sigma_Y \times bt^2/L_0$, which describe a hexagonal prism in the *abc* stress space - see Fig. 3(A). The infinite extent of the failure prism along the $(1, 1, 1)$ direction implies that the regular honeycomb structure will not collapse under equi–biaxial loading. This is reasonable, since regular hexagonal honeycomb can sustain such loading with purely axial forces, and beam axial plastic collapse is suppressed in the results presented here by assigning infinitesimal thickness to the beams inside the unit cell. By intersecting the cone representing uniaxial stress of arbitrary orientation with the prism corresponding to the failure surface of a regular hexagonal honeycomb, one can obtain a simple relationship for estimating collapse strength of a regular honeycomb under uniaxial loading, σ_c, at any angle θ:

$$(\sigma_c/\sigma_Y)_\theta = \frac{\sqrt{3}}{3\cos\left(2\theta' - \frac{\pi}{6}\right)}(t/L_0)^2 \qquad (3)$$

where θ' is the remainder (positive) of division of θ by $\pi/6$. The collapse strength of regular honeycomb structure under pure shear loading, τ_c, at an angle θ can be similarly found and expressed by

$$(\tau_c/\sigma_Y)_\theta = \frac{\sqrt{3}}{6\cos\left(2\theta'' - \frac{\pi}{6}\right)}(t/L_0)^2 \qquad (4)$$

where θ'' is the remainder (positive) of division of $(\theta - \pi/12)$ by $\pi/6$.

For first order hierarchical honeycombs, based on the numerical investigation just five plastic hinge mechanisms appear to govern collapse of a hierarchical honeycomb for all macroscopic state of loading and for all geometries. The dominant mechanisms of collapse are shown in Table 1. The deformed unit cell is shown by dashed lines and the plastic hinge locations are indicated by red dots. For each deformation pattern an arbitrary piece of the unit cell may be considered 'grounded'. Since the unit cell has threefold symmetry, we do not show the equivalent deformation patterns derived by rotations of $2\pi/3$. Each

Table 1

Dominant mechanisms of plastic collapse for hierarchical honeycombs shown for a structural unit cell which are determined from numerical analysis. The locations of plastic hinge for each mechanism are marked by red bullets. The deformed unit cell walls are shown by dashed lines.

1		$$\|F_i - F_j\| = \frac{\sqrt{3}}{4}\sigma_Y \frac{bt^2}{L_0(0.5 - \gamma)}$$ $$(i, j, k = a, b, c; \ i \neq j; \ i \neq k; \ j \neq k)$$
2		$$\|(F_i - F_j)(1 - \gamma) + 3\gamma F_k\| = 3\sqrt{3}\sigma_Y \frac{bt^2}{L_0}$$ $$(i, j, k = a, b, c; \ i \neq j; \ i \neq k; \ j \neq k)$$
3		$$\|F_i - F_j\| = \sqrt{3}\sigma_Y \frac{bt^2}{L_0\gamma}$$ $$(i, j, k = a, b, c; \ i \neq j; \ i \neq k; \ j \neq k)$$
4		$$\|3\gamma(F_i + F_j - F_k) + (F_j - F_k)(1 - 2\gamma)\| = 4\sqrt{3}\sigma_Y \frac{bt^2}{L_0}$$ $$(i, j, k = a, b, c; \ i \neq j; \ i \neq k; \ j \neq k)$$
5		$$\|(F_i - 2F_j + F_k) - (7F_i - 5F_j + F_k)\gamma\| = 4\sqrt{3}\sigma_Y \frac{bt^2}{L_0}$$ $$(i, j, k = a, b, c; \ i \neq j; \ i \neq k; \ j \neq k)$$

collapse mechanism turns out to be a single degree of freedom bar-hinge mechanism, with only enough hinges to permit deformation. With an expectation that these modes are the only ones to be activated by any loading, we algebraically calculated the external work for each deformation mode under arbitrary loading, and used the equality of external and internal work to give a relation between load components at failure. For arbitrary F_a, F_b, F_c the virtual work equality is most easily derived by considering fixed or instant centers for the loaded, moving substructures. The inner envelope of analytical strength formulae obtained from upper bound analysis coincides with the numerically obtained plastic collapse surface given in

Fig. 3(B). Fig. 2 of the supplemental material illustrates the deformed configurations of the first order honeycomb structure according to the mechanisms given in Table 1.

3.3. Finite element analysis

The finite element method is used here to validate strength estimates from the upper bound expressions and the minimization code. 2D rigid-plastic beam element models of the unit cell were constructed using the finite element software ABAQUS. Each cell wall consisted of 100 elements. These were subjected to external load sets derived from arbitrary states of macroscopic stress. Plastic
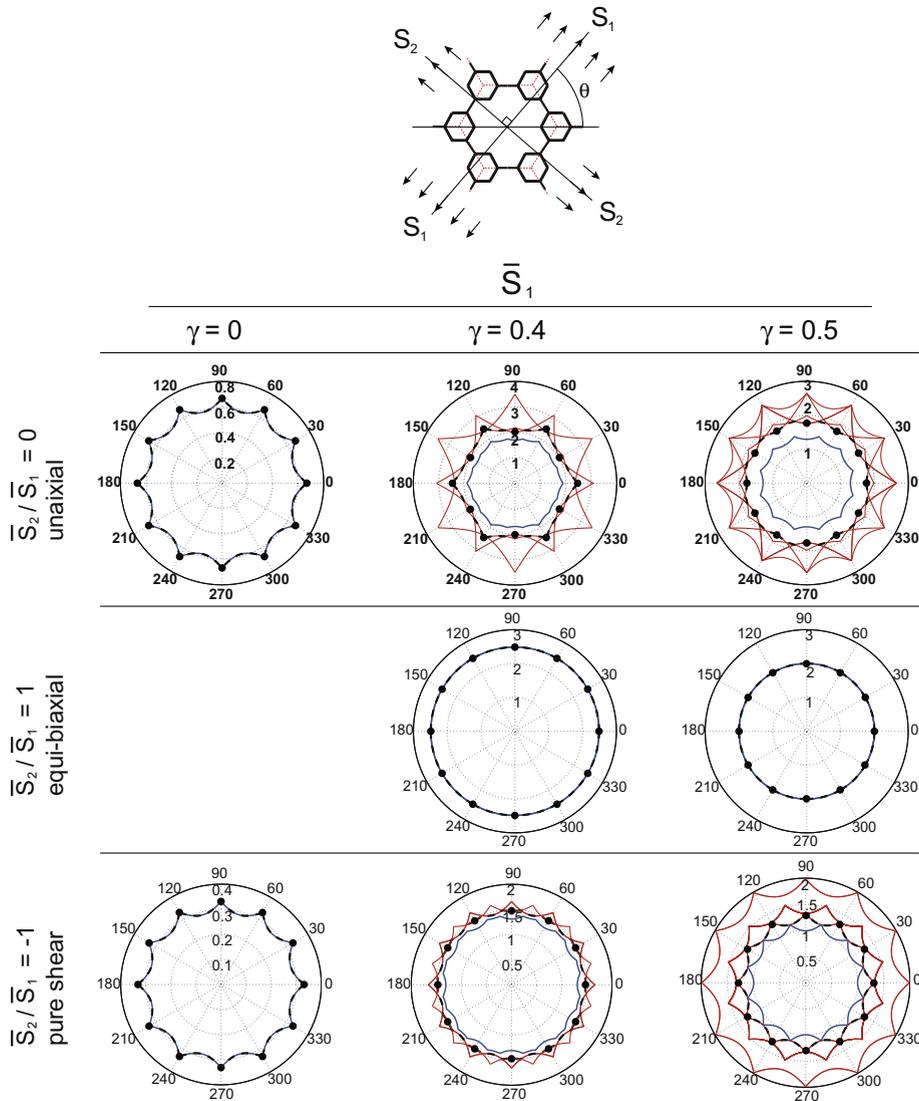
Fig. 4. Plastic collapse maps of regular ($\gamma = 0$) and hierarchical honeycombs ($\gamma = 0.4, 0.5$) for different ratios of principal stresses, $\bar{S}_1$ and $\bar{S}_2$. For each polar plot, the radial value denotes the magnitude of normalized first principal stress, $\bar{S}_1$, causing plastic collapse and the angular value represents the first principal stress angle, θ. The red lines represent the upper bounds of strength from analytical formulae, and the blue line represents a lower bound of strength. The black dashed line shows the strength from the minimization code. The black bullets correspond to the results from finite element analysis. Stresses are normalized according to $\bar{S}_1 = (S_1/\sigma_Y)/(t/L_0)^2$. (For interpretation of the references to color in this figure legend, the reader is referred to the web version of this article.)

collapse under increasing external loads was recognized by large displacements and the failure to converge.

4. Plastic collapse strength under various loadings

Given the bounding algebraic relations between *abc* stress components at failure, the failure condition for any desired state of loading is easily found. Fig. 4 illustrates the normalized value of first principal stress, $\bar{S}_1$, causing plastic collapse as a function of loading direction for three different honeycomb structures under three different ratios of principal stresses, $\bar{S}_2/\bar{S}_1 = 1, 0, -1$. These stress ratios correspond to states of uniaxial, equi-biaxial and pure shear loading, respectively. For each polar plot, the radial value denotes the magnitude of normalized first principal stress, $\bar{S}_1$, causing plastic collapse and the angular value represents the first principal stress angle, θ, as shown in Fig. 4. Stresses are normalized according to $\bar{S}_1 = (S_1/\sigma_Y)/(t/L_0)^2$. The upper bound estimates of strength from analytical formula are shown by red lines, with different lines corresponding to different collapse mechanisms (see the supplemental material for estimations of strength and deformed configurations based on each collapse mechanism.) The inner envelope of the upper bound estimates of strength matches the results from numerical minimization analysis, which is marked by a black dashed line. There is also an agreement between the strength estimates from the finite element analysis, indicated by black bullets, and the minimization analysis. A lower bound estimate for strength is also shown by blue line, which is derived by elastic beam analysis and in which the maximum elastic moment reaches the collapse moment. This is a relatively weak bound because the moment distribution with collapse at multiple points usually does not match the elastic moment distribution. The lower bound estimate of strength is detailed in the supplemental material. For special cases of $\gamma = 0$ or $\bar{S}_1 = \bar{S}_2$ the results from upper and lower bound analyses coincide, therefore the plotted result presents the exact value of plastic collapse. Moreover, the plots of collapse strength versus orientation have a twelvefold symmetry for regular ($\gamma = 0$) and the hierarchical honeycomb with $\gamma = 0.5$. This results in equal plastic collapse strength in *x* and *y* directions. The numerical method can be used to obtain *a full map* of plastic collapse describing the plastic collapse of the lattice structure under various loading conditions. Fig. 5 shows contours for normalized value of first principal stress causing plastic collapse in regular and hierarchical honeycombs ($\gamma = 0.5$) as a function of loading direction, θ, and ratio of principal stresses, $\bar{S}_2/\bar{S}_1$, obtained from upper bound analysis. Taking into account the reflection and rotational symmetries a stress orientation range of $\pi/6$ is sufficient for numerical trials. As the value of $\bar{S}_2/\bar{S}_1$ approaches 1 (equi-biaxial loading) the collapse strength of *regular* honeycomb increases by orders of magnitude since it is stretching-dominated (Gibson et al., 1989; Gibson et al., 1982). However, *hierarchical* honeycombs have a bending-dominated plastic collapse under all states of loading, due to the two-edge nodes in their lattice structure. For plotting the figures, the intersections of cones of fixed principal stress ratio in the *abc* space with the failure surfaces from different mechanisms and the numerical method were obtained as closed curves. The loading intensity at each point on the curve corresponding to a loading direction is proportional to the distance to cone vertex (i.e. origin).

5. Summary and discussion

A numerical scheme is proposed to obtain the plastic collapse mechanism and strength of cellular structures under arbitrary loading conditions. The method minimizes the plastic dissipation inside the unit cell of the structure under given state of loading, and is illustrated for *regular* and *hierarchical* honeycombs. The proposed method is also used to obtain closed-form formulas of plastic collapse strength, enabling us to obtain a comprehensive plastic collapse surface for the lattice structure. Based on an underlying hexagonal network, regular and hierarchical honeycombs have sixfold symmetry in their in-plane properties. For linear properties, such as linear elastic behavior, or thermal conduction along network segments, this means isotropy (Love, 1920), but for nonlinear properties this simply means sixfold symmetry. For the cases of $\gamma = 0$ and $\gamma = 0.5$, however, the failure surface of the material plotted in the *abc* stress state happens to exhibit sixfold symmetry; this results in a twelvefold symmetry in plots of strength versus loading angle. If a lower-symmetry
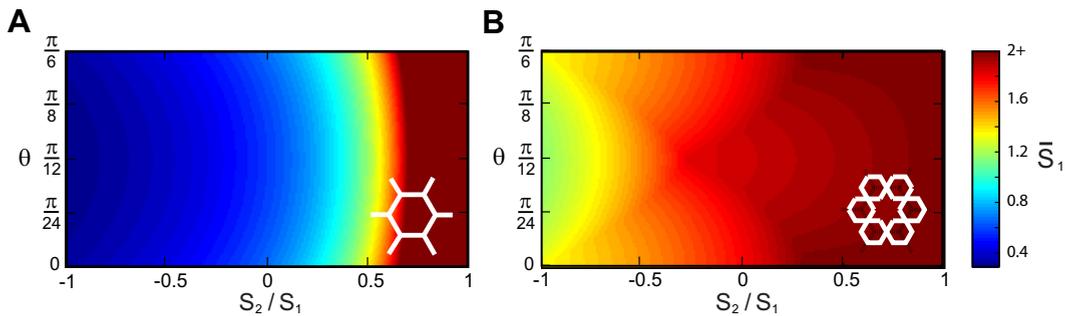

Fig. 5. Contours showing the magnitude of first principal stress causing plastic collapse in a (A) regular, and (B) hierarchical honeycomb ($\gamma = 0.5$) for various ratios of principal stresses, S_1/S_2, and loading direction, θ. Stresses are normalized according to $\bar{S}_1 = (S_1/\sigma_Y)/(t/L_0)^2$.

material is investigated (e.g. a vertically squashed hexagonal network), the same plotting conventions will be informative, although the symmetry will be lost.

The periodic boundary conditions impose no constraints on deformations of the unit cell of regular and hierarchical honeycombs based on the defined geometry of the unit cell in this article. This means that for every arbitrary set of displacements of outer nodes of the unit cell (i.e. nodes 1,4,7 in Fig. 2(B)), a tessellated structure with no gap or beam overlap can be achieved by assembling the unit cells and their 180° rotated counterparts next to each other. When this is the case, simply the minimization of the plastic dissipation function over no constraints is performed. However, for unit cells that are constrained by periodic boundary conditions, the minimization of plastic dissipation inside the unit cell should be performed over the deformation of all (i.e. internal and external) nodes of unit cell which are constrained by periodic boundary conditions on the external nodes (for numerical implementation in MATLAB see help section 'finding the minimum of constrained multivariable functions').

Based on the numerical analyses, the upper bound theorem of plastic collapse provides a more accurate estimation of plastic collapse strength of lattice structures compared to the lower bound theorem. This can be attributed to the possibility of considering multiple-hinged collapse mechanisms for the unit cell in the upper bound analysis as opposed to only one plastic hinge for unit cell in the lower bound analysis. Multiple-hinged collapse mechanisms are most likely the actual mechanisms of collapse for relatively more complex unit cells of lattice structure, as seen for first-order hierarchical honeycomb from the minimization analysis. For a regular honeycomb lattice with only one plastic hinge in its dominant mechanism, the upper bound and lower bound theorems yield identical results under all states of loading. Given the fact that possible mechanisms of collapse for a unit cell of a structure are not mathematically finite, the numerical minimization method discussed in the current work is critical to determine the dominant mechanism(s) of collapse under various loading conditions. The proposed numerical method provides a simple and efficient way to estimate the collapse strength of 2D and 3D lattice structures under a general loading condition, and thus has far reaching implications in designing lightweight and multifunctional structures.

Acknowledgments

Appendix A. Supplementary data

Supplementary data associated with this article can be found, in the online version, at http://dx.doi.org/10.1016/j.mechmat.2013.09.003.

References

Ajdari, A., Haghpanah, B., Papadopoulos, J., Nayeb-Hashemi, H., Vaziri, A., 2012. Hierarchical honeycombs with tailorable properties. International Journal of Solids and Structures 49, 1413–1419.

Ashby, M., 2006. The properties of foams and lattices. Philosophical Transactions of the Royal Society A: Mathematical, Physical and Engineering Sciences 364, 15–30.

Babaee, S., Haghpanah, B., Ajdari, A., Nayeb-Hashemi, H., Vaziri, A., 2012. Mechanical properties of open cell rhombic dodecahedron cellular structures. Acta Materialia 60, 2873–2885.

Chen, W., Han, D., Han, D., 2007. Plasticity for Structural Engineers. J Ross Pub.

Evans, A., Hutchinson, J., Ashby, M., 1998. Multifunctionality of cellular metal systems. Progress in Materials Science 43, 171–221.

Evans, A., Hutchinson, J., Fleck, N., Ashby, M., Wadley, H., 2001. The topological design of multifunctional cellular metals. Progress in Materials Science 46, 309–327.

Gibson, L., Ashby, M., Schajer, G., Robertson, C., 1982. The mechanics of two-dimensional cellular materials. Proceedings of the Royal Society of London A. Mathematical and Physical Sciences 382, 25–42.

Gibson, L., Ashby, M., Zhang, J., Triantafillou, T., 1989. Failure surfaces for cellular materials under multiaxial loads–i modelling. International Journal of Mechanical Sciences 31, 635–663.

Haghpanah, B., Papadopoulos, J., Oftadeh, R., Vaziri, R., 2013. Self-similar hierarchical honeycombs. Proceedings of the Royal Society A 469, 5322–5334.

Jang, W., Kyriakides, S., 2009. On the crushing of aluminum open-cell foams: Part ii analysis. International Journal of Solids and Structures 46, 635–650.

Karagiozova, D., Yu, T., 2004. Plastic deformation modes of regular hexagonal honeycombs under in-plane biaxial compression. International Journal of Mechanical Sciences 46, 1489–1515.

Love, A., 1920. A Treatise on the Mathematical Theory of Elasticity. University Press.

Onck, P., Andrews, E., Gibson, L., 2001. Size effects in ductile cellular solids. Part i: modeling. International Journal of Mechanical Sciences 43, 681–699.

Papka, S., Kyriakides, S., 1994. In-plane compressive response and crushing of honeycomb. Journal of the Mechanics and Physics of Solids 42, 1499–1532.

Zhu, H., Mills, N., 2000. The in-plane non-linear compression of regular honeycombs. International Journal of Solids and Structures 37, 1931–1949.